



Adding Control in Multidisciplinary Design Optimization of a Wing for Active Flutter Suppression

Emmeline Faïsse*, Robin Vernay[†] and Fabio Vetrano[‡]

Airbus Operations SAS, Toulouse, France

Daniel Alazard[§]

ISAE-SUPAERO, Université de Toulouse, Toulouse, France

Joseph Morlier[¶]

ICA, Université de Toulouse, ISAE-SUPAERO, MINES ALBI, UPS, INSA, CNRS, Toulouse, France

Co-design is a multi-disciplinary optimization which aim to concurrently optimize structure and control law. In this work, a co-design method is applied to include a flutter suppression law design in an aeroelastic wing sizing exercise. A nested architecture is used. The outer loop optimizes a beam cross-section and the inner loop is a structured H_∞ synthesis, used to design the flutter control law. The results show the validity of the method, where the model mass is reduced while its flight domain is extended.

I. Introduction

THE design of the next generation of aircraft is driven by efficiency. Aerodynamically, more slender wings with higher aspect ratio are considered for future commercial aircraft. In parallel, structural weight is reduced by using specific composite materials. This will tend to increase the risk of flutter coupling. So, active control and specifically active flutter suppression (AFS) laws must be considered to take credit of these improvements. Including the law design early enough in aircraft design can also increase overall efficiency [1].

AFS research and development started in 1970s and is a fairly developed subject but still not accepted for certification [1]. For this to happen, control laws with proven robustness must be developed. Livne summed up extensively the current state of the art in [1]. The more recent research on AFS laws have been focused on robust law such as H_∞ or H_2 synthesis, μ synthesis or adaptive laws. Classical H_∞ synthesis have been used to control flutter on the mini Multi Utility Technology Testbed (MUTT) as presented by Theis [2] [3] and in the Flexop project [4]. One of the drawbacks of this procedure is that it designs a full order controller, therefore needing a reduction to be implemented. Structured H_∞ synthesis offers a solution by designing a fixed-order controller. Promising results for fixed-order H_∞ control have been shown in [4], [5] and [6].

The design of an active control device is usually done sequentially. First, the structure is optimized then the control law is synthesized for a given structure. However, it has been proven that sequential design is usually not optimal [7]. For AFS, the problem is multi-disciplinary since the wing structure, aeroelasticity and the control law have to be considered. Therefore, multi-disciplinary optimization can be considered to design an optimal wing with AFS. Aeroviscoelastic optimization include active control in aeroelastic wing tailoring. Maneuver or gust load alleviation is often considered such as in [8] but rarely flutter control. One of the few example available is [9] where an active flutter suppression using continuous trailing edge flaps is considered for wing weight minimization.

Integrated structural and control design is a specific multi-disciplinary optimization problem called co-design [10]. Such methodology has been applied by Perez and al. [11] for optimizing satellite payload weight while controlling structural flexible mode. Nash and Jain [12] used co-design to optimize thermal-fluid systems. In the case of wing

*PhD Student, Loads and Aeroelastics, and Institut Clément Ader, emmeline.faisse@airbus.com

[†]Research and Development Engineer, Loads and Aeroelastics

[‡]Research and Development Engineer, Loads and Aeroelastics

[§]Professor, Associate Fellow AIAA

[¶]Professor, Member AIAA

design, Denieul [13] used co-design to size the control surfaces of a blended-wing-body aircraft while meeting the flying quality requirements. Nguyen Van [14] used the same approach based on structured H_∞ design to size the vertical tail, propeller electrical actuator bandwidth and lateral control laws of an electrical aircraft using differential propulsion. However, as mentioned by Livne, concurrent design of wing structure and control law is not yet at its full potential [1]. Integrated design can reach more optimal results in comparison with sequential design but needs caution in the problem definition. The difficulty to apply co-design lies in the lack of multi-disciplinary optimization method that takes into account the dynamic nature of the problem.

Several co-design architectures are presented by Papalambros [10]. They can be linked to MDO architecture as outlined by Allison in [15]. Two strategies which can reach a global optimum are the nested optimization and the simultaneous optimization which can respectively be linked to the multi-discipline feasible (MDF) and the simultaneous analysis and design (SAND) MDO architecture detailed by Martins in [16].

In the nested strategy, an inner loop optimizes the controller while the outer loop optimizes the system. This fits well with optimal and robust control design method which are based on the minimization of a cost function and can therefore be used as the inner loop.

In this paper, this nested architecture is used with a structured H_∞ synthesis as inner optimisation loop. The integrated design loop is applied to a simple test case consisting in a two degrees of freedom aeroelastic airfoil with a control surface augmented with a structural beam model. Control law can easily be designed to actively suppress flutter and applied to the state space model of the airfoil. This test case is a preliminary step to apply the nested methodology design with structured H_∞ design to an industrial wing case.

This paper is organized as follows. First the 2D test case is presented as well as the design method for AFS control law used in the co-design loop. Then, the nested optimization loop is presented and the result on the benchmark case.

II. 2D benchmark case

This section presents the benchmark model used to test out the co-design method for active flutter suppression. It is simple enough so running an optimisation loop does not need long computation time but complex enough exhibit the optimisation characteristics. It is build from a two degree of freedom aeroelastic model, extended with a beam model with thin-walled cross-section.

A. Beam model

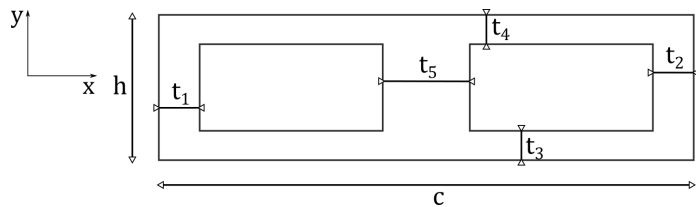


Fig. 1 Thickness parameters t_1, t_2, t_3, t_4 and t_5 of the beam cross-section in the airfoil of width c , height h

The airfoil structure is modeled by a clamped beam with a two-cell thin-walled cross-section to compute the structural parameters for the aeroelastic model. The cross-section is parameterised by five thicknesses: t_1, t_2, t_3 and t_4 model a thin-walled box representing the skin of the wing and the central thickness t_5 defines a solid rectangular section, modeling a central spar. The parametrized cross-section is shown in Figure 1. The height h and the width c of the beam are equal to the height and the chord of the airfoil. The length of the beam is the wing spar. The cross-section filled area is noted A . The beam material is considered as elastic isotropic and defined by ρ its density, E its Young's modulus, G its shear modulus and ν its Poisson's ratio.

The model computes the airfoil mass m , the torsion constant J , the second moments of area I_x, I_y and I_z , the center of gravity position and the moment of inertia I_α at the center of gravity. It also calculates the first bending and torsion frequencies of the beam respectively ω_b and ω_t [17] such that:

$$\omega_b = \sqrt{\left(\frac{1.875}{s}\right)^4 \frac{EI_x}{A\rho}} \text{ and } \omega_t = \frac{\pi}{2s} \sqrt{\frac{GJ}{\rho I_z}}. \quad (1)$$

B. Aeroelastic Model

Outputs from the beam model are used to build a aeroelastic model. The two degrees of freedom of the model are h the plunge displacement and α the pitch angle. The equations of motion of the airfoil are given in (2) [18]. The half chord $\frac{c}{2}$ is noted b .

$$\begin{bmatrix} m & mx_\alpha b \\ mx_\alpha b & I_\alpha \end{bmatrix} \begin{bmatrix} \ddot{h} \\ \ddot{\alpha} \end{bmatrix} + \begin{bmatrix} c_h & 0 \\ 0 & c_\alpha \end{bmatrix} \begin{bmatrix} \dot{h} \\ \dot{\alpha} \end{bmatrix} + \begin{bmatrix} k_h & 0 \\ 0 & k_\alpha \end{bmatrix} \begin{bmatrix} h \\ \alpha \end{bmatrix} = \begin{bmatrix} -L_a \\ M_a \end{bmatrix} \iff \mathbf{M}\ddot{\mathbf{x}}_s + \mathbf{D}_s\dot{\mathbf{x}}_s + \mathbf{K}_s\mathbf{x}_s = \mathbf{f}_{\text{ext}} \quad (2)$$

c_h and c_α are the structural damping. x_α is the non-dimensional distance between the center of gravity C_g and the center of elasticity C_e normalised with respect to b and is shown in Figure 3. The aerodynamic C_l is at a quart chord from the leading edge. a represents the non dimensional distance between the mid-chord M_c and C_e . The structural stiffness are k_h and k_α and equal to:

$$k_h = \omega_b^2 m \text{ and } k_\alpha = \omega_t^2 I_\alpha. \quad (3)$$

$-L_a$ and M_a are the quasi static aerodynamic forces acting on the airfoil and are defined as:

$$\begin{bmatrix} -L_a \\ M_a \end{bmatrix} = 2qb \begin{bmatrix} 0 & -c_{l_\alpha} \\ 0 & -c_{m_\alpha} \end{bmatrix} \begin{bmatrix} h \\ \alpha \end{bmatrix} + \frac{2qb}{V} \begin{bmatrix} -c_{l_\alpha} & -c_{l_\alpha}(\frac{1}{2} - a)b \\ -bc_{m_\alpha} & c_{l_\alpha}(\frac{1}{2} - a)b^2 \end{bmatrix} \begin{bmatrix} \dot{h} \\ \dot{\alpha} \end{bmatrix} + 2qb \begin{bmatrix} c_{l_\beta} \\ c_{m_\beta} \end{bmatrix} \beta = \mathbf{Q}\mathbf{x}_s + \mathbf{Q}_d\dot{\mathbf{x}}_s + \mathbf{Q}_c\beta. \quad (4)$$

V is the free stream velocity. c_{l_α} and c_{m_α} are the lift and moment per angle of attack and c_{l_β} and c_{m_β} are the lift and moment per control surface deflection. They are taken as constant. q is the dynamic pressure, which equals to $\frac{1}{2}\rho_{air}V^2$ where ρ_{air} is the air density.

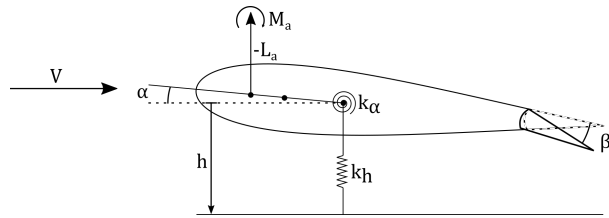


Fig. 2 2D pitch (α) and plunge (h) aeroelastic airfoil model with one control surface (β) subject to aerodynamic forces (M_a and $-L_a$) caused by free stream velocity V .

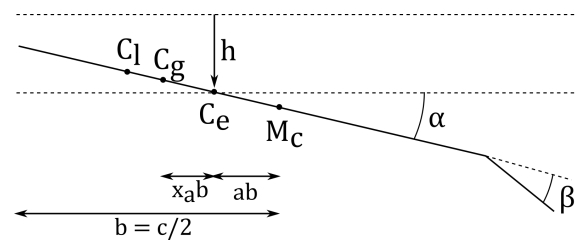


Fig. 3 Airfoil characteristics points C_l , C_g , C_e and M_c and distances b , $x_\alpha b$ and ab .

Equation (2) and (4) are summed up in a state-space system $G(s)$ associated to the state vector:

$$\begin{aligned} \dot{\mathbf{x}} &= \mathbf{Ax} + \mathbf{B}\beta \\ \mathbf{y} &= \mathbf{Cx} + \mathbf{D}\beta \end{aligned} \quad (5)$$

where

$$\mathbf{x} = [h \quad \alpha \quad \dot{h} \quad \dot{\alpha}]^T \quad (6)$$

and

$$\mathbf{A} = \begin{bmatrix} 0 & \mathbf{I}_2 \\ \mathbf{M}^{-1}(\mathbf{Q} - \mathbf{D}_s) & \mathbf{M}^{-1}(\mathbf{Q}_d - \mathbf{K}_s) \end{bmatrix} \text{ and } \mathbf{B} = \begin{bmatrix} 0 \\ \mathbf{M}^{-1}\mathbf{Q}_c \end{bmatrix}, \quad (7)$$

and \mathbf{C} and \mathbf{D} depends on the output needed.

III. Structured H_{∞} for AFS

In this study, the goal is to maintain flutter performance using control even when the airfoil mass m is reduced. A structured H_{∞} synthesis is chosen to design the control law since it has good robustness performance which will be a critical aspect to certify AFS device on commercial aircrafts.

The H_{∞} synthesis is realised using systune from Matlab R2018b. The design requirements are given as Soft Goals and Hard Goals, which are respectively the objectives and the constraints of the synthesis. Detailed explanation of the structured H_{∞} process are given in [19].

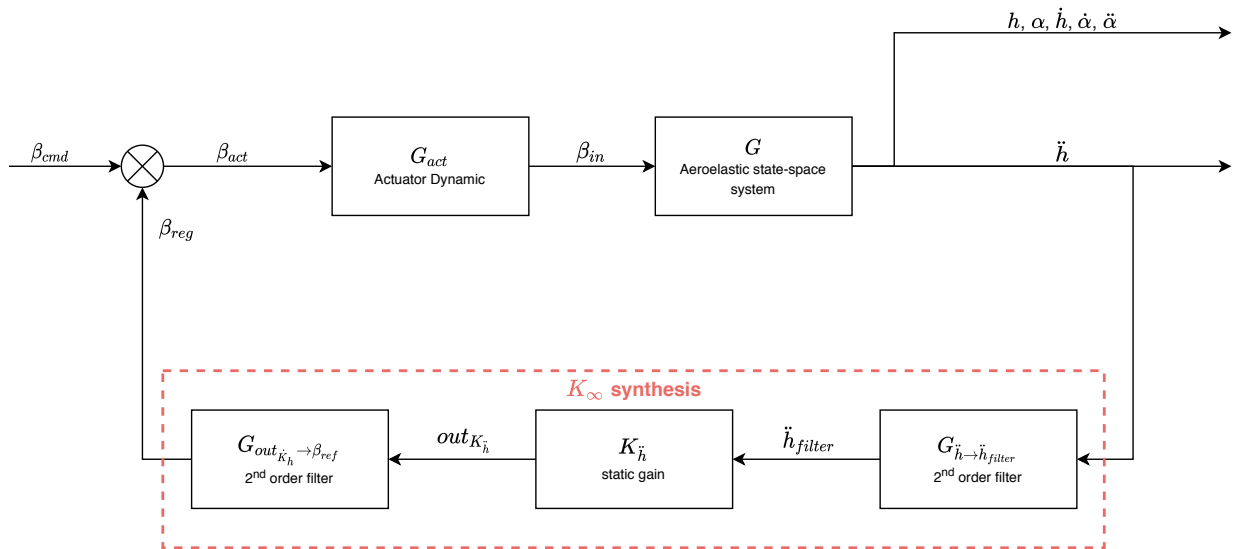


Fig. 4 Flowchart for structured H_{∞} synthesis

The system flowchart is shown in Figure 4. Accelerometers are the usual sensors on wings and given the simplicity of the model, only one sensor measuring vertical acceleration \ddot{h} is considered. The feedback loop output is the regulated control surface angle β_{reg} .

The actuator dynamic is modeled with a second order low pass filter with a cutoff frequency ω_{act} of 100 rad/s. Its transfer function G_{act} is detailed in (8). It is an unrealistic high rate but necessary given the model frequencies.

$$G_{act}(s) = \frac{\omega_{act}^2}{s^2 + \sqrt{2}\omega_{act}s + \omega_{act}^2} \quad (8)$$

The feedback loop is built using three blocks with fixed structure. The overall filter is noted K_{∞} . The design variable of the H_{∞} synthesis are the coefficients of the filters. They are updated by the optimisation algorithm while keeping the overall order of the filter.

The first block is initialised as a notch filter centered on the structural bending frequency ω_b . It is a second order filter which transfer function is $G_{\ddot{h} \rightarrow \ddot{h}_{filter}}$ in (9).

$$G_{\ddot{h} \rightarrow \ddot{h}_{filter}}(s) = \frac{s^2 + 0.02\omega_b s + \omega_b^2}{s^2 + 0.14\omega_b s + \omega_b^2} = \frac{a_1 s^2 + b_1 s + c_1}{a_2 s^2 + b_2 s + c_2} \quad (9)$$

The second block is a static gain noted $K_{\ddot{h}}$ and the third one is initialised as a band-pass filter to suppress possible high and low frequency instabilities. Its transfer function $G_{out_{K_h} \rightarrow \beta_{ref}}$ is given in (10).

$$G_{out_{K_h} \rightarrow \beta_{ref}}(s) = \frac{s + 1}{s^2 + 14s + 100} = \frac{b_3 s + c_3}{a_4 s^2 + b_4 s + c_4} \quad (10)$$

Overall, $K_{\ddot{h}}$ and the $[a_i, b_i, c_i]$ are the 12 design variables of the synthesis.

Once the global structure of the controller is set up, the soft and hard goals for the H_∞ have to be defined. The goal of the controller is to keep the aeroelastic system stable until a given speed. In the optimization, this velocity will be chosen depending on the initial structure flutter speed. For now, it will be noted V_f .

The speed is taken as an uncertain parameter for the system. Therefore the H_∞ synthesis will try to stabilize the system, under the requirements, for all velocities from 0 to $1.2V_f$. In practice, the range for which the controller is optimized is reduced to $[0.8V_f, 1.2V_f]$, assuming that until $0.8V_f$ the aeroelastic system is stable.

The first requirement is the objective function and is applied to $T_{\beta_{cmd} \rightarrow \ddot{h}}(s)$ the closed loop transfer between β_{cmd} and \ddot{h} , as seen in Figure 4, for frequencies between 1 and 100 rad/s. Its goal is to flatten the peaks in open loop frequency response shown in Figure 5. Since its a soft goal, the optimizer will minimize the distance between the weight function and the system transfer function. The frequency domain template $W_{\beta_{cmd} \rightarrow \ddot{h}}$ is also depicted in Figure 5 and reads:

$$W_{\beta_{cmd} \rightarrow \ddot{h}} = \left(\frac{\omega_b s}{s + \omega_b} \right)^2. \quad (11)$$

The two other requirements are constraints and must be enforced for the optimizer to converge. The second goal (Req. 2) is a pole position enforcement. The pole of the closed loop system must be in the left half plane in a domain $\mathcal{D}(\xi_l, \omega_l)$, shown in Figure 6, defined by a minimum damping ratio of $\xi_l = 10^{-4}$ and a maximum frequency of $\omega_l = 2\omega_t$.

The last goal (Req. 3) constrains the frequency domain response of the controller $K_\infty(s)$ in order to limit the control surface deflection. The weight function is $W_{\ddot{h} \rightarrow \beta_{reg}}$ detailed in (12) and its plot is in Figure 7.

$$W_{\ddot{h} \rightarrow \beta_{reg}} = \frac{1}{s + 1} \quad (12)$$

Once the H_∞ synthesis designed the feedback loop, the closed-loop system will be noted CL and its flutter speed V_{CL}^f . The control design problem is summed up in (13), where $\tilde{\sigma}(.)$ is the highest singular value, $\lambda_i(.)$ is the i -th pole and $n = 10$ is the order of the closed-loop system. Equation (13a) is the mathematical representation of Req. 1, (13b) of Req.2 and (13c) of Req. 3.

$$(13) \quad \forall V \in [0.8V_f, 1.2V_f], \begin{cases} \{\widehat{K}_{\ddot{h}}, \widehat{a}_i, \widehat{b}_i, \widehat{c}_i\} = \min_{K_{\ddot{h}}, a_i, b_i, c_i} \max_{\omega \in [1, 100] \text{ (rad/s)}} \tilde{\sigma} \left(\frac{1}{W_{\beta_{cmd} \rightarrow \ddot{h}}(j\omega)} T_{\beta_{cmd} \rightarrow \ddot{h}}(j\omega) \right) & (13a) \\ \text{such that } \lambda_i(T_{\beta_{cmd} \rightarrow \ddot{h}}(s)) \in \mathcal{D}(\xi_l, \omega_l), \forall i = 1, \dots, n, & (13b) \\ \tilde{\sigma}(K_\infty(j\omega)) < |W_{\ddot{h} \rightarrow \beta_{reg}}|, \forall \omega & (13c) \end{cases}$$

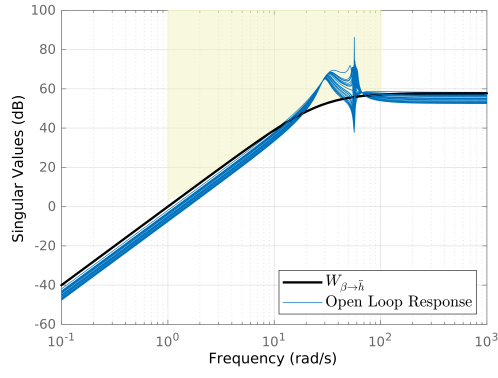


Fig. 5 Frequency domain template $W_{\beta_{cmd} \rightarrow \bar{h}}$ (Req. 1) and open loop response for speed in $[0.8V_f, 1.2V_f]$, outlining the two structural modes $w_h = 27.8$ rad/s and $w_\alpha = 56.6$ rad/s

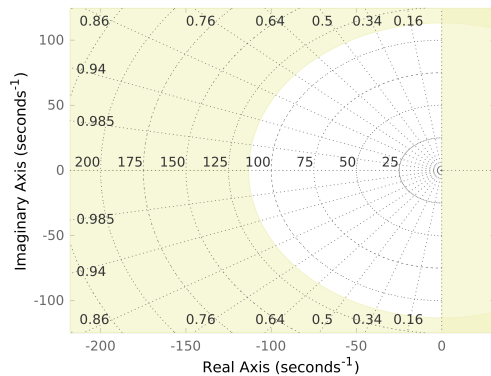


Fig. 6 Pole domain $\mathcal{D}(\xi_l, \omega_l)$ constraint in white for Req. 2

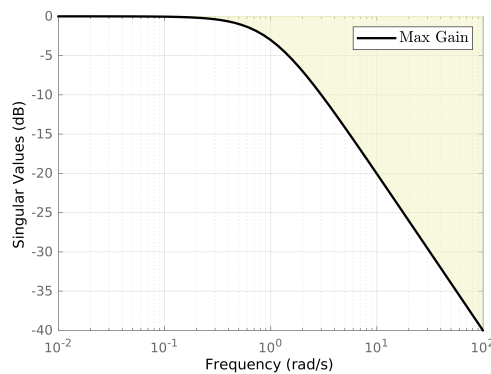


Fig. 7 Req. 3 weight function $W_{\bar{h} \rightarrow \beta_{reg}}$

IV. Optimization

A nested optimisation architecture or multi-discipline feasible (MDF) is chosen for two main reasons. Firstly, H_∞ synthesis is already an optimisation process. Therefore, it is easier to include a control design loop inside the structural optimisation process than to mix them. Moreover, Matlab robust control tools offer numerous possibilities for H_∞ synthesis but works as a black box once the optimisation is launched. It is then difficult to access data to make it run in an individual discipline feasible (IDF) optimisation loop. Secondly, keeping structural and control optimisation process separated makes it easier to consider using the architecture for optimizing a finite element larger scale wing.

The nested architecture is made of one outer optimisation loop, which corresponds to the structural optimisation and one inner loop which is the H_∞ synthesis. For each computation of the outer loop objective, an inner loop optimisation is run to design the control law. A graphic description of the process is presented in Figure 8. f_{out} and f_{in} are respectively the objective function of the outer and the inner loop, g_j^{out} and g_i^{in} the constraints and x_S and x_C the design variables.

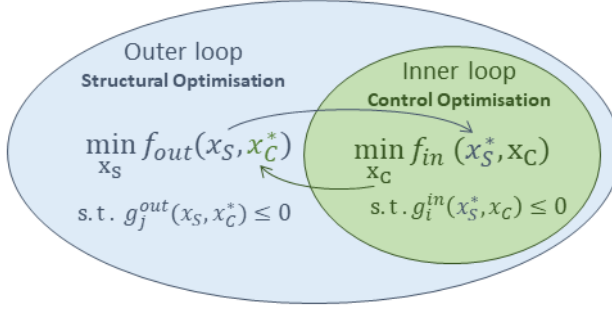


Fig. 8 Nested optimisation architecture

The optimisation objective is to reduce airfoil mass while keeping the flutter performance of the initial wing. The outer loop optimisation is detailed in (14). The objective function (14a) is defined as a trade-off between the mass and the flutter speed. V_{ref} and M_{ref} are reference values to normalize the speed and the mass, usually taken as the initial point flutter speed and mass. w_1 and w_2 are weights that can be used to plot a Pareto frontier (see Section V) or place penalty on one or the other objective.

The structural design variables x_S are the thickness parameters of the cross-section t_1, t_2, t_3, t_4 and t_5 . Equation (14b) refers to the solving of state space (5). The control design variables x_C are the design variables of the H_∞ synthesis and are presented in (13), as well as the inner objective function f_{in} in (13a) and the constraints g_i^{in} in (13b) and (13c). This is summed up in (14c). The boundary conditions on x_S are enforced through (14e) and are geometrically defined limits, such as detailed in Section II.A.

$$(14) \left\{ \begin{array}{l} \min_{x_S, x_C} f_{obj} = w_1 \frac{m(\mathbf{x}_S)}{m_{ref}} - w_2 \frac{V_{CL}^f(\mathbf{x}_S, \mathbf{x}_C)}{V_{ref}} \\ \text{subject to aeroelastic equilibrium (function of } \mathbf{x}_S \text{)} \\ \quad \text{converged inner loop (13) (function of } \mathbf{x}_S \text{ and } \mathbf{x}_C \text{) for } [0.8V_{OL}^f(\mathbf{x}_S), 1.2V_{ref}] \\ \quad 1 - \frac{V_{CL}^f}{V_{ref}} \leq 0 \\ \quad \mathbf{x}_S^{\text{LB}} < \mathbf{x}_S < \mathbf{x}_S^{\text{UB}} \end{array} \right. \begin{array}{l} (14a) \\ (14b) \\ (14c) \\ (14d) \\ (14e) \end{array}$$

One non linear constraint g_1^{out} is defined in (14d) which ensure that the flutter speed in closed loop stays at least equal or above the flutter speed in open loop of the initial wingbox. In the case the inner loop fails to design a controller matching the inner loop constraints, the last converged x_C which satisfies the outer loop constraints is kept. This keeps the flutter performance unaltered in the worst case, or greater than initially in better cases.

The outer loop optimisation is run using patternsearch function from Matlab R2018b, with mesh and constraint tolerance set to 10^{-4} .

V. Results

The co-design methodology is tested using the aeroelastic model presented in Section II.B and the H_∞ synthesis from Section III. The wing dimension and material are adapted from the Goland wing [20]. The parameters that are constant during the optimisation are presented in Table 1.

Wing Dimension		Material Parameters	
s	6.096 m	ρ	38.2723 kg/m ³
c	1.829 m	E	1.2062.10 ⁸ N
h	0.5 m	ν	0.29
a	0.3	G	8.044.10 ⁶ N

Table 1 Constant parameters

	Starting point	Lower Bound	Upper Bound
t_1	$\frac{c}{15}$	$\frac{c}{20}$	$\frac{c}{10}$
t_2	$\frac{c}{15}$	$\frac{c}{20}$	$\frac{c}{10}$
t_3	$\frac{h}{15}$	$\frac{h}{20}$	$\frac{h}{10}$
t_4	$\frac{h}{15}$	$\frac{h}{20}$	$\frac{h}{10}$
t_5	$s - 2\frac{c}{10}$	0	$s - 2\frac{c}{10}$

Table 2 Initial design variables and boundaries

The initial cross-section is chosen as quasi full and its thickness parameters are given in Table 2 as well as the boundaries on the structural design variables. They are chosen so the thin-wall approximation will stay valid for the outside walls throughout the optimisation and the central wall will not over overlap the side walls. The mass and open loop flutter speed of the optimisation starting point are given in Table 3 , and and outline of the initial cross-section is plotted in Figure 9.

Initial Mass	Initial V_{OL}^f
201 kg	158.5 m/s

Table 3 Optimisation starting point values



Fig. 9 Starting point cross-section outline

73 optimisations are run with 73 different weights couple (w_1, w_2) distributed between 0 and 1 and such that $w_2 = 1 - w_1$. The results are summed up in the Pareto front plotted in Figure 10. Several weight couples can lead to the same final result, therefore less than 73 mass and closed loop flutter speed couples are attained.

The optimisation result where $w_1 = 1$ and $w_2 = 0$ is represented in Figure 10. This case represents a design where only the mass is minimised while the flutter speed is not included in the global objective. It is analog to an iterative sequential design method. From Figure 10, it is seen that this case is neither the best in mass reduction nor in flutter performance and it is not close the Pareto front. It proves the benefit of co-design for active flutter suppression.

Three results on the extrapolated Pareto front are examined more closely and their final values are given in Table 4. Outline of the third case final cross-section is plotted for example in Figure 11.

Figures12 and 13 shows the frequency response for the three cases plotted against the requirements template. Figure 12 shows the peak attenuation in closed loop for the three cases in comparison to the open loop frequency response at V_{OL}^f . The feedback frequency response for the three cases is plotted in Figure 13. It shows that the feedback globally attenuates the \ddot{h} output with a higher gain around the torsion frequency in order to control this mode. This is represen-

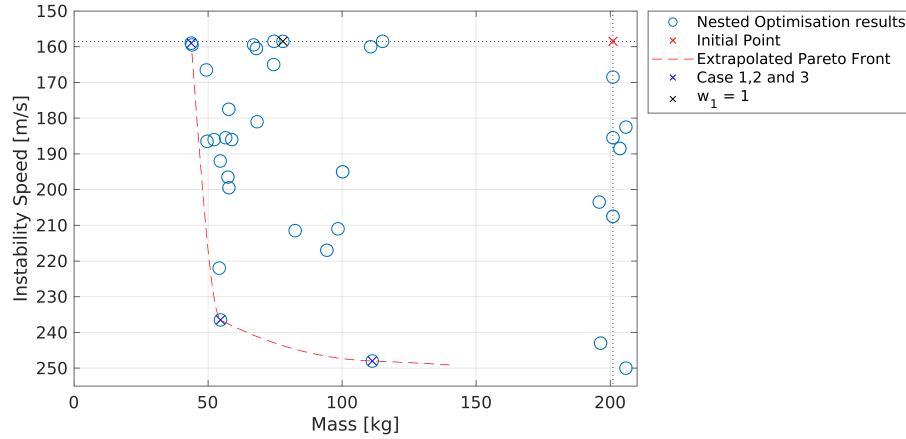


Fig. 10 Optimisation results for 73 objective function weights with Case 1 ($m = 43.73 \text{ kg}$, $V_{OL}^f = 159 \text{ m/s}$), Case 2 ($m = 54.64 \text{ kg}$, $V_{OL}^f = 236.5 \text{ m/s}$) and Case 3 ($m = 111.3 \text{ kg}$, $V_{OL}^f = 248 \text{ m/s}$) outlined.

	Final Mass	Final V_{CL}^f	Mass Gain
Case 1	43.73 kg	159 m/s	78.2 %
Case 2	54.64 kg	236.5 m/s	72.8 %
Case 3	111.30 kg	248 m/s	44.7 %

Table 4 Initial design variables and boundaries



Fig. 11 Case 3 final cross-section outline

tative of the behavior of K_∞ which is the multiplication of $G_{\ddot{h} \rightarrow \ddot{h}_{filter}}$, $K_{\ddot{h}}$ and $G_{out_{K_h} \rightarrow \beta_{ref}}$ for all optimisation results.

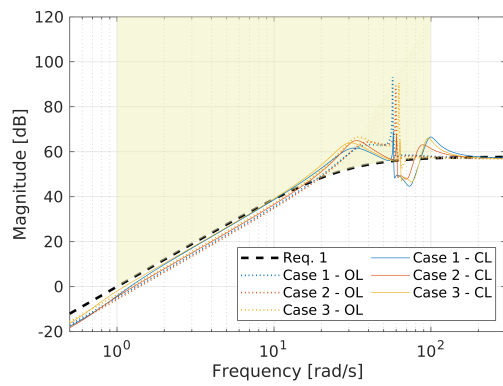


Fig. 12 Comparison of $T_{\beta_{cmd} \rightarrow \ddot{h}}$ in open loop and closed loop for Case 1, 2 and 3 at V_{OL}^f

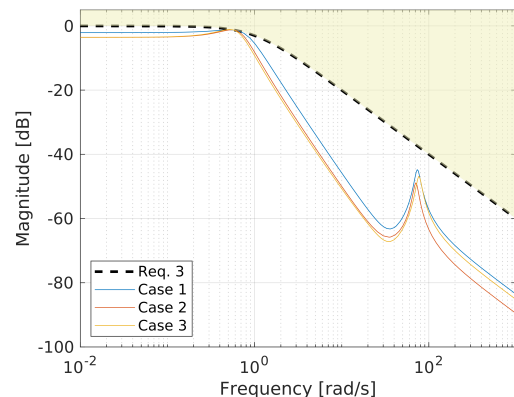


Fig. 13 K_∞ frequency response for Case 1, 2 and 3

Figure 14 shows the flutter plot for the three cases final airfoil design. They all show that the controller reduce the bending mode (in red) damping in closed loop while keeping the torsion mode damping (in blue) positive, with a margin of at least 0.01% for all velocity between 0 and 250 m/s. The mode frequencies in closed loop are close to the one in open loop and do not exhibit divergence.

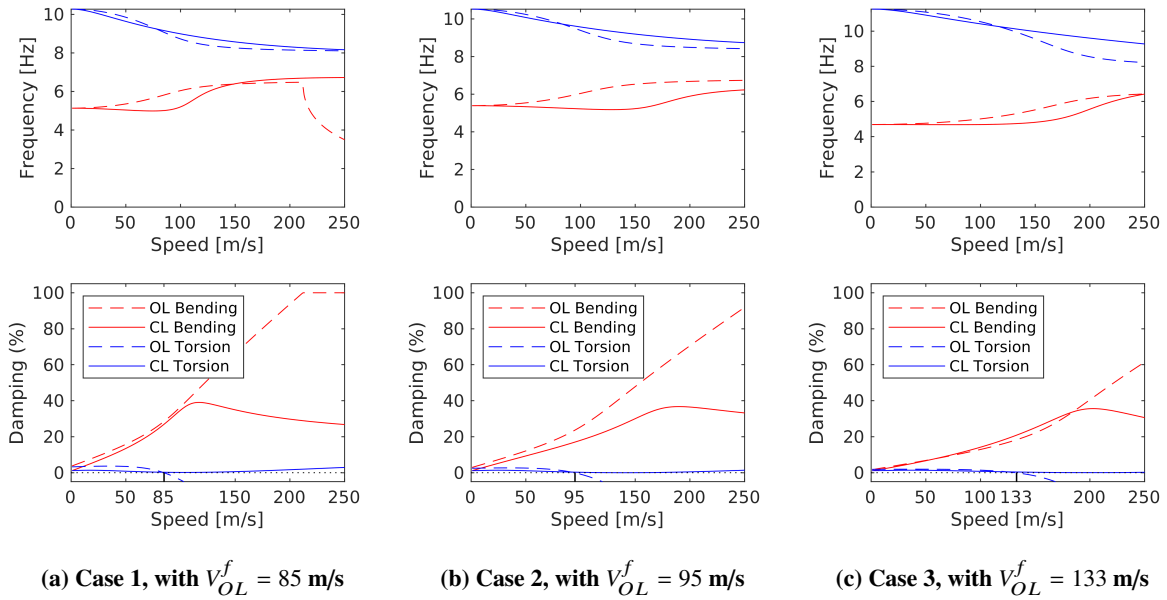


Fig. 14 Frequency and damping of structural modes for velocity range between 0 and 250 m/s

However, looking at Figure 15, 17 and 18, it can be seen that there is an instability coming from control modes at respectively 159 m/s, 237 m/s and 248 m/s for case 1, 2 and 3. The controller is designed for a velocity range between $0.8V_{OL}^f$ (respectively 68 m/s, 75.6 m/s and 106 m/s) and $1.2V_{ref} = 190.2 \text{ m/s}$. Therefore the synthesis cannot guarantee the system stability over $1.2V_{ref}$ when converged and $V_{ref} = 158.5 \text{ m/s}$ if the inner loop fails to converge, as mentioned in Section IV. The controller does stabilize the structural modes until V_{ref} , however it fails to be itself stable over this velocity. It is too efficient regarding flutter but lacks robustness. There is possibility to improve the controller design process to avoid its instability. The initial goal was to keep the instability speed at least equal to V_{ref} and this condition is respected.

Figure 16a shows the comparison between open loop and closed loop pitch and plunge time response for a 1° angle of attack input at open loop flutter speed for case 1 and Figure 16b the control surface angle time evolution. The closed loop response is not divergent but it is not significantly damped and exhibits oscillations. Their frequency is around 8.5 Hz. The actuator bandwidth was also set high to be able to control the structural frequencies of the airfoil. On foreseen commercial aircraft, first wing first structural modes are usually under 3 Hz there actuators should need less bandwidth.

Adaptation of the control design is necessary to transpose the methodology to a real aircraft case and would include more sensors and actuators, as well as other constraints such as comfort constraints in the control design loop or buckling constraints on the wing structure. However, the feasibility of a nested co-design architecture with a structured H_∞ synthesis as an inner loop has been proven on the 2D benchmark case and promising results in comparison with sequential design have been shown.

VI. Conclusion

This paper presents a nested co-design architecture to design concurrently structure and control law and a structured H_∞ synthesis for active flutter suppression. The methodology is applied to a 2D aeroelastic airfoil benchmark case, augmented with a beam structural model. The co-design method is made of an outer loop which optimises the structural mass of the airfoil while preserving the flutter performance, the H_∞ synthesis as an inner loop. Results outline that a co-design method give better results than a sequential method. The 2D test case was a preliminary step before applying the methodology to finite element 3D wing. First, improvements on the control law for flutter suppression have to be made but first results are promising for the next step.

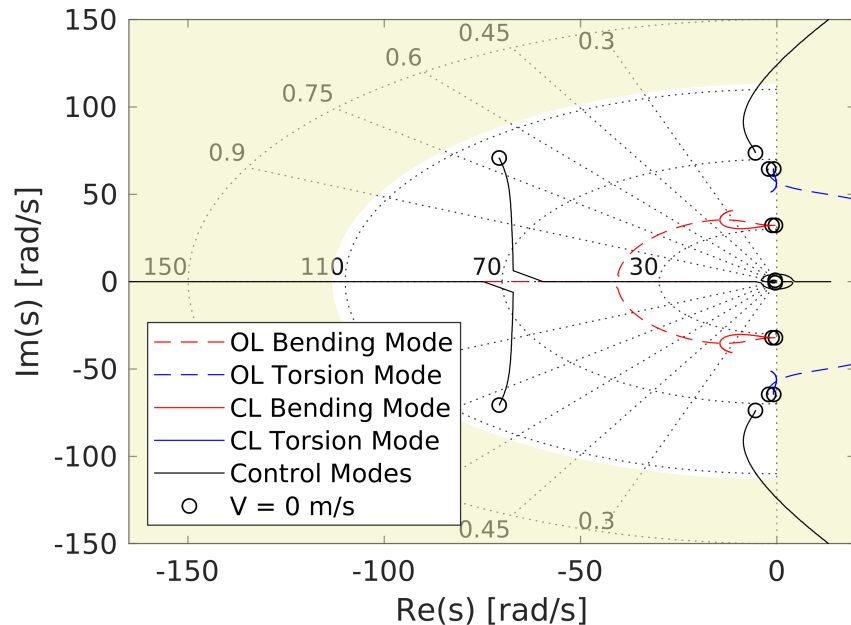


Fig. 15 Pole evolution with speed for CL and OL systems for Case 1, with velocity from 0 to 250 m/s

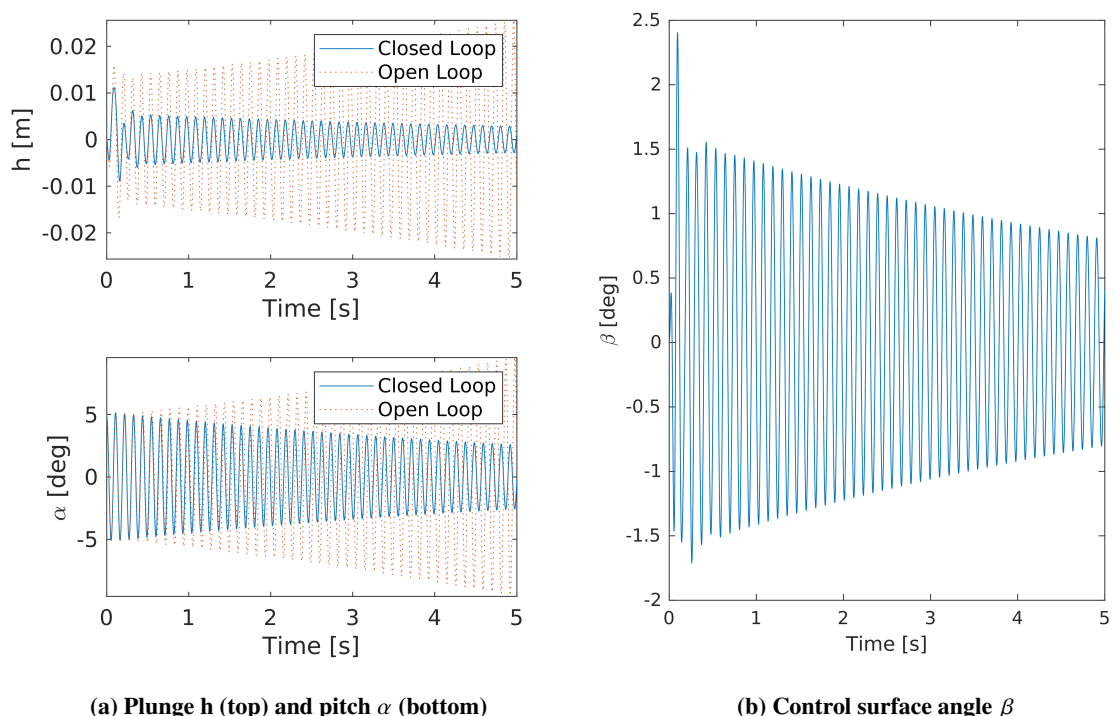


Fig. 16 Response to a 1° change in angle of attack at speed $V_{OL}^f + 1 \text{ m/s} = 86 \text{ m/s}$ for Case 1

Appendix

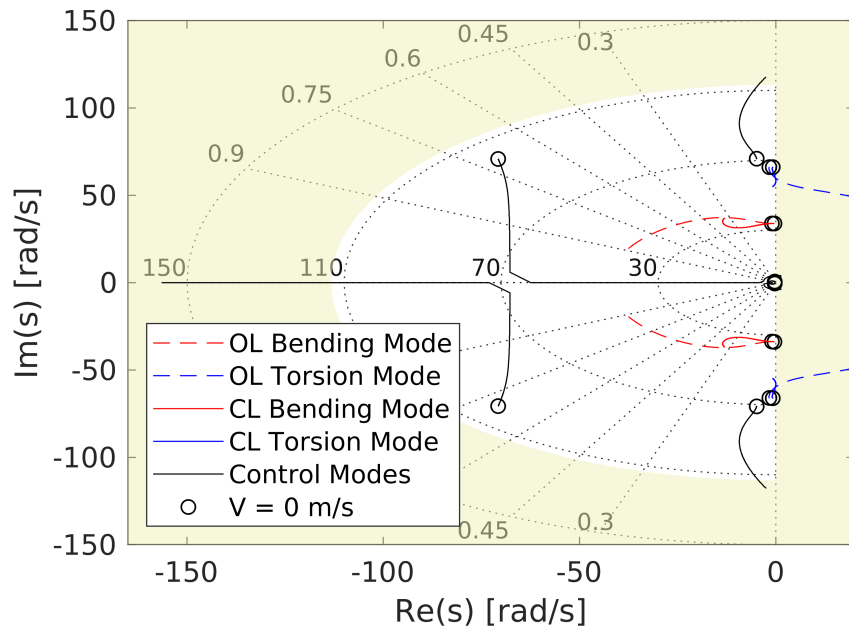


Fig. 17 Pole evolution with speed for CL and OL systems for Case 2, with velocity from 0 to 250 m/s

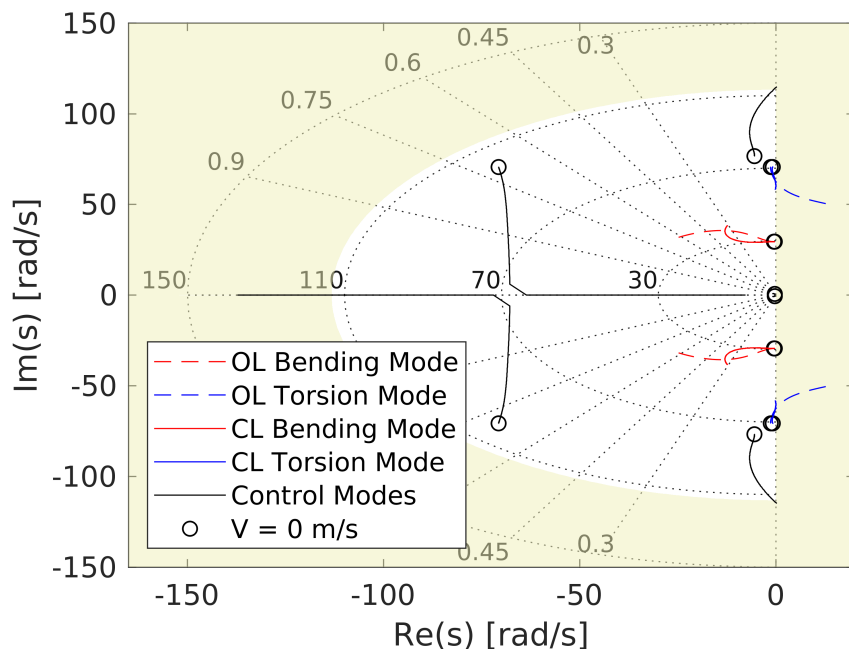


Fig. 18 Pole evolution with speed for CL and OL systems for Case 1, with velocity from 0 to 250 m/s

References

- [1] Livne, E., "Aircraft Active Flutter Suppression: State of the Art and Technology Maturation Needs," *Journal of Aircraft*, Vol. 55, No. 1, 2018, pp. 410–452. <https://doi.org/10.2514/1.C034442>.
- [2] Theis, J., Pfifer, H., and Seiler, P., "Robust Control Design for Active Flutter Suppression," *AIAA Atmospheric Flight Mechanics Conference*, San Diego, California, USA, 2016.
- [3] Theis, J., Pfifer, H., and Seiler, P., "Robust Modal Damping Control for Active Flutter Suppression," *Journal of Guidance, Control, and Dynamics*, Vol. 43, No. 6, 2020, pp. 1056–1068. <https://doi.org/10.2514/1.G004846>.
- [4] Waitman, S., and Marcos, A., "Active flutter suppression: non-structured and structured Hinfinity design," *IFAC-PapersOnLine*, Vol. 52, No. 12, 2019, pp. 146–151. <https://doi.org/10.1016/j.ifacol.2019.11.184>.
- [5] Svoboda, F., and Hromcik, M., "Active flutter suppression by means of fixed-order Hinfinity control: results for the Benchmark Active Control Technology (BACT) wing," *18th European Control Conference (ECC)*, Naples, Italy, 2019, pp. 119–124. <https://doi.org/10.23919/ECC.2019.8795733>.
- [6] Lhachemi, H., Saussie, D., and Zhu, G., "Flutter Suppression for a Two Degree of Freedom Aeroelastic Wing Section: a Structured H-infinity-Based Gain-Scheduling Approach with Explicit Hidden Coupling Terms Handling," *AIAA Guidance, Navigation, and Control Conference*, 2013. <https://doi.org/10.2514/6.2017-1735>.
- [7] Allison, J. T., Guo, T., and Han, Z., "Co-Design of an Active Suspension Using Simultaneous Dynamic Optimization," *Journal of Mechanical Design*, Vol. 136, No. 8, 2014. <https://doi.org/10.1115/1.4027335>.
- [8] Haghigat, S., Martins, J. R. R. A., and Liu, H. H. T., "Aeroservoelastic Design Optimization of a Flexible Wing," *Journal of Aircraft*, Vol. 49, No. 2, 2012, pp. 432–443. <https://doi.org/10.2514/1.C031344>.
- [9] Stanford, B. K., "Static and Dynamic Aeroelastic Tailoring with Variable-Camber Control," *Journal of Guidance, Control, and Dynamics*, Vol. 39, No. 11, 2016, pp. 2522–2534. <https://doi.org/10.2514/1.G000413>.
- [10] Papalambros, P. Y., and Wilde, D. J., *Principles of Optimal Design: Modeling and Computation*, 3rd ed., Cambridge University Press, 2017. <https://doi.org/10.1017/9781316451038>.
- [11] Alvaro Perez, J., Pittet, C., Alaward, D., and Loquen, T., "Integrated Control/Structure Design of a Large Space Structure using Structured H_∞ Control," *IFAC-PapersOnLine*, Vol. 49, No. 17, 2016, pp. 302 – 307. <https://doi.org/10.1016/j.ifacol.2016.09.052>.
- [12] Nash, A. L., and Jain, N., "Combined Plant and Control Co-Design for Robust Disturbance Rejection in Thermal-Fluid Systems," *IEEE Transactions on Control Systems Technology*, 2019, pp. 1–8.
- [13] Denieul, Y., Bordeneuve, J., Alazard, D., Toussaint, C., and Taquin, G., "Multicontrol Surface Optimization for Blended Wing-Body Under Handling Quality Constraints," *Journal of Aircraft*, Vol. 55, No. 2, 2018, pp. 638–651. <https://doi.org/10.2514/1.C034268>.
- [14] Van, E. N., Alazard, D., Döll, C., and Pastor, P., "Co-design of aircraft vertical tail and control laws using distributed electric propulsion," *IFAC-PapersOnLine*, Vol. 52, No. 12, 2019, pp. 514–519. <https://doi.org/10.1016/j.ifacol.2019.11.295>.
- [15] Allison, J. T., Guo, T., and Han, Z., "Co-Design of an Active Suspension Using Simultaneous Dynamic Optimization," *Journal of Mechanical Design*, Vol. 136, No. 8, 2014. <https://doi.org/10.1115/1.4027335>.
- [16] Martins, J. R. R. A., and Lambe, A. B., "Multidisciplinary Design Optimization: A Survey of Architectures," *AIAA Journal*, Vol. 51, No. 9, 2013, pp. 2049–2075. <https://doi.org/10.2514/1.J051895>.
- [17] Banerjee, J., "Explicit Frequency Equation and Mode Shapes of a Cantilever Beam Coupled in Bending and Torsion," *Journal of Sound and Vibration*, Vol. 224, No. 2, 1999, pp. 267–281. <https://doi.org/10.1006/jsvi.1999.2194>.
- [18] Ko, J., Kurdila, A. J., and Strganac, T. W., "Nonlinear Control of a Prototypical Wing Section with Torsional Nonlinearity," *Journal of Guidance, Control, and Dynamics*, Vol. 20, No. 6, 1997, pp. 1181–1189. <https://doi.org/10.2514/2.4174>.
- [19] Gahinet, P., and Apkarian, P., "Structured Hinfinity synthesis in MATLAB," *18th IFAC World Congress*, Vol. 18, 2011, pp. 1435–1440.
- [20] Goland, M., "The Flutter of a Uniform Cantilever Wing," *Journal of Applied Mechanics*, Vol. 12, No. 4, 1945, p. A197–A208.